Research Square

Preprints are preliminary reports that have not undergone peer review.
They should not be considered conclusive, used to inform clinical practice,
or referenced by the media as validated information.

Atherosclerosis and Diabetic Foot Share a Common Molecular Signature of Cellular Senescence: A Multi-Omics and Machine Learning Study

Fuguang Zhang
General Hospital of Southern Theater Command
Heng Wang
Shenzhen Second People's Hospital
Yuelu Yang
Zhujiang Hospital
Changhong Li
Zhujiang Hospital
Xuejun Weng
General Hospital of Southern Theater Command
Tao Zhang
Guangzhou Medical University
Jianwu Chen
chenjianwu5@126.com

General Hospital of Southern Theater Command

Research Article

Keywords: cellular senescence, atherosclerosis, diabetic foot ulcer, machine learning, CALCOCO1, CCND2, FUCA1, metformin

Posted Date: November 1st, 2026

DOI: https://doi.org/10.21203/rs.3.rs-11347381/v1

License: This work is licensed under a Creative Commons Attribution 4.0 International License.
Read Full License

Additional Declarations: No competing interests reported.

Abstract

Atherosclerosis (AS) and diabetic foot ulcer (DFU) are two major vascular complications of diabetes that frequently co-exist, yet whether they share a common molecular basis remains unclear. Here, we tested the hypothesis that AS and DFU share a common senescence-related molecular signature. We integrated transcriptomic datasets GSE134431 (DFU) and GSE163154 (AS), identified differentially expressed genes common to both diseases, and intersected them with the CellAge senescence-associated gene set to obtain senescence-related DEGs (SR-DEGs). Three machine learning algorithms—LASSO, random forest, and SVM-RFE—were applied to prioritize core feature genes, which were subsequently validated at the single-cell (GSE245703), tissue, and in vitro levels. We identified 72 SR-DEGs shared by AS and DFU, from which three core feature genes—CALCOCO1, CCND2, and FUCA1—were selected by cross-algorithm consensus. A multi-gene nomogram incorporating these genes achieved excellent discriminative performance in both diseases (AUC: 0.96 for DFU, 0.90 for AS). Single-cell analysis revealed cell type–restricted expression patterns of these genes, with fibroblasts emerging as a key senescent cell type in the DFU microenvironment. Clinical validation in an independent cohort of 22 patients (11 DFU vs. 11 non-diabetic foot ulcer) confirmed significant accumulation of senescent cells and dysregulated feature gene expression in DFU tissues. Moreover, metformin treatment effectively attenuated hydrogen peroxide- and high-glucose/high-lipid-induced fibroblast senescence in vitro, partially reversing the expression changes of the three feature genes. These findings demonstrate that AS and DFU share a common senescence-associated molecular signature, identify CALCOCO1, CCND2, and FUCA1 as potential diagnostic and therapeutic targets, and suggest that metformin may exert protective effects through modulation of this senescence-related gene network.

Introduction

Atherosclerosis (AS) and diabetic foot ulcer (DFU) are two major vascular complications of diabetes that frequently co-exist and share a poor prognosis[1][2][3]. A large Swedish cohort study of 655,250 patients with type 2 diabetes demonstrated a 2.59-fold increased risk of lower extremity artery disease and a 1.69-fold increased risk of extracranial large artery disease[4]. This striking epidemiological overlap strongly suggests the existence of shared pathophysiological drivers underlying these two seemingly distinct conditions.

Both AS and DFU arise from the same metabolic soil—chronic hyperglycemia, dyslipidemia, and insulin resistance[5][6]. These metabolic disturbances create a pro-oxidative and pro-inflammatory microenvironment that drives endothelial dysfunction in AS and microvascular insufficiency in DFU—two vascular pathologies that converge on a common cellular denominator: the accumulation of senescent cells in the vessel wall and wound bed[7][8]. Mechanistically, the same metabolic stressors—elevated glucose, oxidized lipids, and advanced glycation end-products—activate the p53/p21 and p16/Rb senescence pathways in both vascular smooth muscle cells (AS) and dermal fibroblasts (DFU) [9][10][11]. Consequently, senescent cells accumulate in both atherosclerotic plaques and diabetic wound tissues,

where their senescence-associated secretory phenotype (SASP) perpetuates local inflammation and impairs tissue repair[12][13][14][15]. Crucially, despite the distinct cellular contexts—vascular smooth muscle cells and macrophages in AS versus fibroblasts and keratinocytes in DFU—these two diseases converge on a shared functional outcome: SASP-driven establishment of a pro-inflammatory, tissue-destructive microenvironment that destabilizes plaques in AS and impairs wound closure in DFU. This convergence on a common functional consequence raises the central question of whether a core senescence program is shared across these distinct cellular contexts.

Despite this conceptual overlap, previous investigations have largely examined AS and DFU in isolation. A systematic evaluation of whether these two diabetic complications share a common senescence-related molecular signature—and whether such a shared signature could account for their frequent clinical coexistence—remains conspicuously lacking.

To address this gap, we tested the hypothesis that AS and DFU share a common molecular basis rooted in cellular senescence. We integrated public transcriptomic datasets using cross-dataset normalization strategies, applied machine learning algorithms to filter noise and identify robust shared genes, and mapped their cell-type-specific expression via single-cell RNA sequencing. Furthermore, given metformin's well-established anti-senescent properties through AMPK activation, we used it as a pharmacological probe to assess the functional relevance of our identified signature in an in vitro fibroblast senescence model. Through this cross-disease integrative framework, we aim to uncover a systemic senescence network underlying diabetic vasculopathies and to offer potential molecular targets for simultaneous risk stratification and therapeutic intervention.

Results

1. Cellular senescence represents a common pathological hallmark of both diabetic foot and atherosclerosis

Transcriptomic profiling of DFU (GSE134431) and AS (GSE163154) tissues identified 2,510 and 1,815 differentially expressed genes (DEGs), respectively, with 408 genes commonly dysregulated in both diseases (Fig. 1e). Functional enrichment revealed convergence on lysosomal function, phagosome maturation, and PPAR signaling, as well as cytoskeletal reorganization and extracellular matrix remodeling—canonical features of the senescence-associated secretory phenotype (SASP) (Fig. 1c, d). Intersecting these 408 shared DEGs with the CellAge senescence-associated gene set yielded 72 senescence-related DEGs (SR-DEGs) (Fig. 1f), which were significantly enriched in lysosomal acidification, oxidative stress responses, and oxidative phosphorylation (Fig. 1g, h), further reinforcing the pivotal role of cellular senescence in DFU–AS comorbidity.

2. Machine learning prioritizes three core feature genes by cross-algorithm consensus

To identify the most representative feature genes from the 72 SR-DEGs, we employed three machine learning algorithms. LASSO regression with 10-fold cross-validation identified 6 hub genes with non-zero

coefficients at the optimal penalty parameter (Fig. 2a, b). Random forest (RF) analysis, based on mean decrease Gini ranking, identified 36 potential biomarkers (Fig. 2c, d). Support vector machine-recursive feature elimination (SVM-RFE) identified 8 key genes (Fig. 2e). Intersection of the genes identified by all three algorithms yielded three core feature genes: CALCOCO1, CCND2, and FUCA1 (Fig. 2f), which were selected for subsequent analysis.

3. A multi-gene nomogram achieves robust discriminative performance in both diseases

ROC curve analysis demonstrated that each of the three feature genes showed good individual discriminative ability in both disease settings. In the DFU dataset (GSE134431), the AUC values for CALCOCO1, CCND2, and FUCA1 were 0.845, 0.803, and 0.864, respectively; in the AS dataset (GSE163154), the corresponding AUC values were 0.923, 0.963, and 0.900, respectively (Fig. 3a, b).

To enable individualized risk quantification, we constructed a multi-gene diagnostic nomogram integrating the three feature genes for predicting DFU or AS probability (Fig. 3c, d). The combined model exhibited excellent discriminative performance, with AUC values of 0.96 (95% CI: 0.879–1.000) in the DFU dataset and 0.90 (95% CI: 0.825–0.999) in the AS dataset (Fig. 3e, h). Decision curve analysis confirmed that clinical decisions guided by this nomogram would yield net benefit across a range of threshold probabilities (Fig. 3f, i). Calibration curves further demonstrated good concordance between predicted probabilities and observed outcomes in both cohorts (Fig. 3g, j). Of note, the wider confidence interval observed in the AS dataset is likely attributable to its limited sample size, highlighting the need for further validation in larger, independent cohorts. Collectively, these findings position the three-gene nomogram as a promising risk stratification tool for DFU and AS comorbidity, while also providing supportive evidence for the shared molecular basis hypothesis.

4. Feature genes display cell type–specific expression patterns within diabetic foot tissue

Single-cell RNA sequencing of skin specimens from DFU patients (GSE245703), coupled with stringent quality filtering and batch effect correction, yielded 158,641 high-quality single-cell transcriptomes, and unsupervised clustering based on canonical marker gene expression resolved 14 distinct cell populations (Fig. 4a, b). Comparative analysis of cellular composition revealed significantly increased proportions of fibroblasts, macrophages, and monocytes, accompanied by a marked reduction in keratinocytes (Fig. 4c, d), indicating that fibroblasts together with immune populations constitute the most prominently altered compartments within the DFU microenvironment; given their substantial enrichment and established roles in extracellular matrix turnover and wound remodeling, fibroblasts were selected as the relevant cell model for subsequent in vitro studies. Examination of feature gene distribution across cell types uncovered distinct expression patterns: CALCOCO1 was predominantly enriched in fibroblasts and pericytes (Fig. 4e, h), CCND2 was primarily expressed in keratinocytes, basal cells, and fibroblasts (Fig. 4f, i), and FUCA1 showed high expression in macrophages and fibroblasts (Fig. 4g, j), suggesting that these three genes are likely engaged in DFU pathogenesis via distinct molecular pathways operating in a cell type–dependent manner.

5. Senescent cells accumulate in diabetic foot ulcer tissues

A total of 22 participants were enrolled, including 11 DFU patients and 11 nDFU controls, with no significant differences in age or sex distribution (Table 1). Compared with nDFU controls, DFU patients exhibited significantly higher blood glucose (8.19 ± 2.80 vs. 4.85 ± 0.56 mmol/L, $P < 0.001$) and inflammatory markers, including ultrasensitive C-reactive protein (47.95 ± 32.12 vs. 8.03 ± 10.23 mg/L, $P < 0.001$) and serum amyloid A (401.24 ± 547.9 vs. 32.97 ± 51.99 mg/L, $P = 0.038$), along with reduced hemoglobin (101.68 ± 18.40 vs. 131.82 ± 20.62 g/L, $P = 0.002$), albumin (32.83 ± 4.30 vs. 40.89 ± 3.04 g/L, $P < 0.001$), and albumin-to-globulin ratio (1.04 ± 0.21 vs. 1.52 ± 0.35, $P = 0.001$). Renal function parameters were elevated, including blood urea nitrogen (7.82 ± 2.81 vs. 4.54 ± 1.43 mmol/L, $P = 0.003$) and cystatin C (1.53 ± 0.46 vs. 0.98 ± 0.27 mg/L, $P = 0.003$), while lymphocyte percentage was markedly lower in DFU patients (15.94 ± 7.59% vs. 26.03 ± 10.72%, $P = 0.019$), consistent with systemic inflammation, nutritional impairment, and immune dysfunction.

Histological analysis confirmed these clinical observations. DFU tissues showed larger ulcer areas, delayed healing, marked structural disorganization, and increased inflammatory infiltration (Fig. 5a). Immunohistochemistry revealed significantly higher proportions of cells positive for p21, γH2AX, and HMGB1, as well as increased SA-β-gal-positive cells, compared with nDFU tissues (Fig. 5b, c; $P < 0.05$). Both p16 and p21 were significantly upregulated at the protein and transcript levels (Fig. 5d, e; $P < 0.05$), and canonical SASP components (IL-1β, IL-6, MMP1, MMP3, and TNF-α) were consistently overexpressed in DFU lesions (Fig. 5f; $P < 0.05$). Quantitative RT-PCR further confirmed that CCND2 was significantly upregulated, whereas CALCOCO1 and FUCA1 were downregulated in DFU tissues (Fig. 5g; $P < 0.05$), fully consistent with the expression patterns in GSE134431 (Fig. 5h; $P < 0.05$). Collectively, these data demonstrate substantial senescent cell accumulation in DFU tissues, validating the bioinformatics predictions and reinforcing the link between diabetic foot pathology and cellular senescence.

Table 1| Clinical characteristics of nDFU and DFU patients.

This table summarizes the demographic, blood routine, inflammatory markers, and biochemical parameters of non-diabetic foot ulcer (nDFU) and diabetic foot ulcer (DFU) patients. Data are presented as mean ± SD for continuous variables and as counts for categorical variables (gender). Comparisons between groups were performed using Student's t-test for normally distributed continuous variables or the Mann–Whitney U test for non-normally distributed variables, and Fisher's exact test for categorical variables. Statistical significance is indicated by *$P < 0.05$. Abbreviations: WBC, white blood cell; RBC, red blood cell; M, male; F, female.

Variables	nDFU(n=11)	DFU(n=11)	P value
Gender(M/F)	7/4	6/5	0.999
Age (years)	61.27±9.561	63.83±8.747	0.5096
WBC count (10^9/L)	8.370±3.434	10.37±4.597	0.2611
Neutrophil count (10^9/L)	5.636±3.592	7.980±4.327	0.5669
Lymphocyte count (10^9/L)	1.933±0.7016	1.493±0.5458	0.1163
Monocyte count (10^9/L)	0.5127±0.2183	0.5736±0.1852	0.4885
Eosinophil count (10^9/L)	00.2148±0.1820	0.1809±0.1091	0.6048
Basophil count (10^9/L)	0.03818±0.02483	0.04455±0.01864	0.5044
Neutrophil rate (%)	62.63±15.35	67.26±20.86	0.5596
Lymphocyte rate (%) *	26.03±10.72	15.94±7.590	0.0192
Monocyte rate (%)	6.909±2.787	5.959±2.276	0.3916
Eosinophil rate (%)	3.927±3.729	2.117±1.443	0.1489
Basophil rate (%)	0.5091±0.3239	0.4873±0.3580	0.8824
RBC count (1012/L) *	4.400±0.6534	3.191±0.4145	<0.0001
Hemoglobin (g/L) *	131.8±20.62	101.6±18.40	0.0017
Ultrasensitive C-reactive protein (mg/L) *	8.025±10.23	47.95±32.12	0.0008
Serum Amyloid A (mg/L) *	32.97±51.99	401.2±547.9	0.0382
Total Protein (g/L)	68.54±6.031	65.73±5.769	0.2775
Albumin (g/L) *	40.89±3.044	32.83±4.300	<0.0001
Globulin (g/L) *	26.69±5.252	34.00±4.911	0.0030
Albumin-to-Globulin Ratio*	1.520±0.3493	1.036±0.2064	0.0008
Blood Glucose (mmol/L) *	4.849±0.5644	8.189±2.803	0.0009
Blood Urea Nitrogen (mmol/L) *	4.544±1.431	7.815±2.808	0.0026
Creatinine (μmol/L)	68.09±19.44	87.18±34.48	0.1254
Uric Acid (μmol/L) *	321.6±69.46	448.0±179.1	0.0412
Cystatin C (mg/L) *	0.9827±0.2651	1.529±0.4602	0.0028
Total Bilirubin (μmol/L)	12.16±3.897	8.700±3.858	0.0591
Alanine Aminotransferase (U/L)	18.27±7.226	17.18±6.691	0.7172
Alkaline Phosphatase (U/L)	90.64±37.45	75.55±21.15	0.2583
Gamma-Glutamyl Transferase (U/L)	25.36±9.750	19.36±7.284	0.1177
Alpha-L-Fucosidase (U/L)	17.91±5.205	16.09±3.807	0.3609

Note: *$p < 0.05$

6. Metformin alleviates fibroblast senescence in a diabetic-like microenvironment in vitro

To evaluate metformin's effect on senescence in diabetic wound healing, we established an in vitro fibroblast senescence model using primary human dermal fibroblasts exposed to H_2O_2 or high-glucose/high-lipid (HGHL), which mimic diabetic wound oxidative and metabolic stress. These treatments significantly increased SA-β-gal-positive cells (Fig. 6a, b) and upregulated p21 and p16 mRNA (Fig. 6c, e; $P < 0.05$), confirming a senescence-like phenotype; metformin treatment significantly reduced SA-β-gal-positive cells and attenuated p21 and p16 expression (Fig. 6a, b; 6c, e; $P < 0.05$). Additionally,

H_2O_2 or HGHL upregulated CCND2 and downregulated CALCOCO1 and FUCA1, and these changes were partially reversed by metformin (Fig. 6d, f; $P < 0.05$). Together, these findings suggest that metformin attenuates fibroblast senescence in a diabetic-like microenvironment, potentially by modulating a regulatory network involving CCND2, CALCOCO1, and FUCA1.

Discussion

This study identifies a shared senescence signature underlying diabetic foot and atherosclerosis. Functional enrichment and machine learning pointed to CALCOCO1, CCND2, and FUCA1 as core diagnostic biomarkers, with fibroblasts playing a key role in the diabetic foot senescent microenvironment. Clinical tissue validation confirmed significant accumulation of senescent cells and dysregulated expression of these feature genes in diabetic foot ulcer tissues. In vitro experiments further demonstrated that metformin alleviates fibroblast senescence induced by oxidative or metabolic stress, partially reversing the expression changes of CALCOCO1, CCND2, and FUCA1.

Atherosclerosis and diabetic foot ulcer represent two distinct manifestations of diabetic vascular disease that differ fundamentally in their primary cellular players—vascular smooth muscle cells and macrophages in AS versus fibroblasts and keratinocytes in DFU. Despite this cellular divergence, they share a common pathological trajectory: chronic metabolic stress drives cellular senescence in both tissue compartments, and the resulting SASP establishes a local pro-inflammatory milieu that perpetuates tissue dysfunction. Our transcriptomic analysis revealed that the 408 commonly dysregulated genes between AS and DFU converged significantly on pathways central to senescence—lysosomal function, phagosome maturation, and PPAR signaling (Fig. 1c, d)—suggesting that these two diseases, despite their distinct anatomical and cellular contexts, are linked by a core senescence-associated molecular program.

Enrichment of shared DEGs in senescence-related pathways implicates cellular senescence as a key hub connecting vascular pathologies. This inference was directly validated in DFU tissue, which showed significantly increased proportions of cells positive for senescence markers p21, γH2AX, HMGB1, and SA-β-gal, along with upregulated SASP factor expression. These observations align with previous findings in atherosclerotic plaques, where senescent foam cells drive local inflammation and plaque instability through SASP[16], and vascular smooth muscle cell senescence promotes atherosclerosis progression and plaque vulnerability[17]. By connecting observations from two independent fields, our study proposes "vascular senescence" as a potential common contributor for diabetic vascular complications, providing a unified framework for understanding systemic vascular damage in diabetic patients.

Single-cell transcriptomic analysis revealed marked heterogeneity in cellular senescence within DFU tissue. Increased proportions of fibroblasts and macrophages, coupled with decreased keratinocytes, suggest profound remodeling of the cellular microenvironment. Cell type-specific expression patterns of feature genes—CALCOCO1 and CCND2 upregulated in DFU-derived fibroblasts, FUCA1 downregulated in

both macrophages and fibroblasts—indicate that senescence of different cell types may contribute to DFU pathogenesis through distinct molecular mechanisms. Fibroblasts, as primary executors of wound healing, upon senescence exhibit reduced extracellular matrix synthesis and impaired remodeling capacity while disrupting the local immune microenvironment via SASP, hindering macrophage polarization toward the reparative M2 phenotype[18]. Keratinocyte senescence affects re-epithelialization efficiency, delaying wound coverage. Macrophage senescence impairs phagocytic function and promotes excessive inflammatory factor release, further aggravating local tissue damage. These findings align with the emerging view that cellular senescence in chronic wounds is a multicellular process involving multiple cell types[19].

The three feature genes identified in this study showed consistent expression trends across independent datasets, clinical samples, and cellular models, suggesting they play important regulatory roles in diabetic foot senescence.

CCND2, a key positive regulator of the G1/S transition, was upregulated in DFU tissue. This is consistent with the paradoxical observation that senescent cells, despite being cell cycle-arrested, often show persistent or even increased expression of cyclins. CCND2 appears to play a complex role in stress-induced senescence. Transient upregulation may represent a compensatory attempt to re-enter the cell cycle, whereas sustained high expression may activate CDK4/6, initiating pRB phosphorylation and engaging crosstalk with the p16-pRB and p53/p21-dependent senescence programs[20][21]. Recent studies have implicated the PRC2.1 complex in epigenetic regulation of CCND2[22]. Importantly, CCND2 accumulation in late-stage senescent fibroblasts depends on functional p21[23], suggesting that CCND2 upregulation is a consequence, rather than a cause, of senescence execution. Specific upregulation of CCND2 in diabetic foot fibroblasts is consistent with this model, positioning CCND2 as a marker of the senescence process in the diabetic wound microenvironment.

CALCOCO1, an autophagy receptor protein involved in selective clearance of ubiquitinated protein aggregates and damaged organelles[24], was downregulated in DFU tissue, particularly in fibroblasts. This suggests impaired autophagic function. Autophagy and senescence are closely interconnected: functional autophagy clears damaged proteins and mitochondria accumulated in senescent cells, delaying cellular senescence; conversely, impaired autophagy accelerates senescence and enhances SASP release[25]. The recently proposed "autophagy-senescence axis threshold model" further elucidates this dynamic balance: below a damage threshold, autophagy inhibits senescence initiation; beyond the threshold, autophagy is reprogrammed to support the metabolic demands of senescent cells, including SASP production[26]. Under diabetic conditions, high glucose has been shown to inhibit fibroblast autophagy, leading to reduced collagen synthesis and delayed wound healing[27]. Thus, CALCOCO1 downregulation may reflect defective autophagy in DFU tissue, promoting fibroblast senescence and impairing wound healing.

FUCA1, encoding lysosomal alpha-L-fucosidase, was downregulated in DFU tissue, primarily in macrophages and fibroblasts. Lysosomal dysfunction is a hallmark of cellular senescence; senescent cells exhibit increased lysosomal volume but decreased degradation efficiency, manifested as elevated SA-β-gal activity[28]. FUCA1 downregulation may lead to accumulation of fucosylated substrates in lysosomes, aggravating lysosomal dysfunction and promoting maintenance of the senescent phenotype. Fucosylation itself participates in cell adhesion, signal transduction, and immune regulation, and its metabolic abnormalities may contribute to SASP regulation by affecting intercellular communication[29]. FUCA1 downregulation in macrophages may be particularly significant, as macrophage phagocytic function and inflammatory regulatory capacity depend on an intact lysosomal system.

The three feature genes identified in this study converge on three interconnected pillars of the senescence machinery: autophagic clearance (CALCOCO1), cell cycle regulation (CCND2), and lysosomal homeostasis (FUCA1). We propose that these pillars operate in a coordinated manner in the pathogenesis of both AS and DFU.

First, impaired autophagy, reflected by CALCOCO1 downregulation, compromises the removal of damaged mitochondria and protein aggregates—a process critically important in both lipid-laden foam cells of atherosclerotic plaques and metabolically stressed fibroblasts of diabetic wounds. Second, lysosomal dysfunction, reflected by FUCA1 downregulation, impairs the degradative capacity of senescent cells, contributing to the accumulation of SASP components that perpetuate local inflammation. Third, the paradoxical upregulation of CCND2—despite cell cycle arrest—suggests an aborted attempt at mitotic re-entry, a hallmark of stressed cells in both vascular and cutaneous compartments.

This autophagy–lysosome–cell cycle triad provides a mechanistic framework that transcends the generic concept of “cellular senescence” and offers a disease-relevant molecular vocabulary for understanding the shared vulnerability of arteries and diabetic skin to chronic metabolic stress. Importantly, this framework also suggests that therapeutic strategies targeting any one of these three pillars—autophagy enhancement, lysosomal restoration, or cell cycle modulation—may have beneficial effects across both disease contexts.

Metformin's ability to alleviate fibroblast senescence provides new mechanistic insights into its protective effects[30][31]. Metformin has been shown to delay multi-organ aging and extend healthspan in non-human primate models[32]. In vascular cells, metformin activates AMPK, inhibits mTOR signaling, and enhances autophagic function, alleviating oxidative stress and inflammation-induced senescence[33]. In our study, metformin treatment reduced senescent cell proportion and p16/p21 expression while upregulating CALCOCO1 expression, suggesting that metformin may ameliorate the senescent state by restoring autophagic function—consistent with CALCOCO1's role as an autophagy receptor. Metformin's regulation of CCND2 and FUCA1 expression further suggests coordinated modulation of cell cycle, lysosomal function, and autophagy pathways through a multi-target network. These results corroborate findings that miR-181b-5p regulates endothelial cell senescence through the

Nrf2/HO-1 pathway[34], collectively suggesting the central role of the senescence regulatory network in diabetic wound healing.

The multi-gene diagnostic model based on CALCOCO1, CCND2, and FUCA1 exhibited good discriminatory efficacy in both DFU and AS (AUC 0.96 and 0.90, respectively). Calibration curves and decision curve analysis confirmed its clinical applicability. This model may enable early diagnosis of DFU and risk stratification for systemic vascular complications in diabetic patients. Given the high comorbidity of DFU and AS, a molecular tool capable of simultaneously assessing risk for both diseases holds potential clinical value—facilitating early identification of potential coronary artery disease risk in diabetic foot patients and enabling more aggressive comprehensive intervention strategies. Moreover, feature gene expression patterns and their modulation by metformin offer new avenues for developing anti-aging-based therapeutic strategies for diabetic foot.

While our experimental validation focused on DFU tissues due to sample availability, substantial evidence from the literature supports the relevance of the three feature genes to AS pathogenesis. CCND2 has been implicated in vascular smooth muscle cell proliferation and phenotypic switching, key events in atherogenesis[20]. CALCOCO1-mediated autophagy has been shown to regulate lipid metabolism in macrophage foam cells, and its dysfunction promotes atherosclerotic plaque progression[24]. FUCA1, though less studied in AS, regulates lysosomal function in vascular endothelial cells under glycative stress[29]. Collectively, these published findings—together with our transcriptomic data from GSE163154 confirming differential expression of all three genes in AS tissues—support the translational relevance of the three-gene signature to AS, although direct experimental validation in human AS tissues remains a priority for future investigations.

Several limitations should be acknowledged. First, while our transcriptomic analysis identified a shared senescence signature between AS and DFU, experimental validation of the three feature genes in AS tissues—ideally through immunohistochemistry and qPCR on human atherosclerotic plaques—remains to be completed. We have, however, provided supportive evidence from published literature and from the GSE163154 dataset to substantiate the relevance of these genes to AS pathogenesis. Second, the bioinformatics analysis relies on public databases with inherent heterogeneity in sample sources and processing methods; the diagnostic model requires validation in large, prospective, independent cohorts. Third, specific functional mechanisms of CALCOCO1, CCND2, and FUCA1 in cellular senescence remain to be fully elucidated; gene knockout/overexpression experiments are needed to establish causal roles in fibroblast senescence and wound healing. Fourth, the upstream signaling network through which metformin regulates feature gene expression requires systematic investigation, particularly the role of the AMPK-mTOR-autophagy axis. Finally, the complexity of human diabetic foot pathology, including infection and neuropathy, necessitates validation in models that more closely recapitulate clinical conditions. Despite these limitations, our study provides a hypothesis-generating framework for understanding the shared senescence biology of AS and DFU and offers testable predictions for future mechanistic and translational studies.

This study provides evidence for a common molecular basis of cellular senescence underlying diabetic foot and atherosclerosis, identifies CALCOCO1, CCND2, and FUCA1 as core feature genes, and constructs an effective comorbidity diagnostic model. It further validates senescent cell accumulation in clinical tissues and provides preliminary in vitro evidence that metformin exerts anti-senescent effects in fibroblasts. Future in vivo studies are needed to confirm these findings and to assess the therapeutic potential of metformin in diabetic foot.

Methods

Data Acquisition and Processing

Transcriptomic datasets for DFU (GSE134431) and AS (GSE163154) were obtained from the Gene Expression Omnibus (GEO) database. The single-cell RNA-seq dataset GSE245703 (skin tissue from 7 nDFU patients and 5 DFU patients) was also downloaded from GEO. A list of senescence-associated genes was retrieved from the CellAge database (https://genomics.senescence.info/cells/). All raw expression data were log2-transformed and quantile-normalized. For microarray datasets, probe IDs were mapped to gene symbols using the corresponding platform annotation files; multiple probes for the same gene were collapsed by taking the mean expression value.

Differential Expression and Functional Enrichment Analysis

Differentially expressed genes (DEGs) were identified using dataset-specific pipelines. For the GSE134431 dataset, DEGs were analyzed using the DESeq2 package in R, with significance thresholds set at $|\log_2 \text{fold change}| > 1$ and adjusted $P < 0.05$. For the GSE163154 dataset, DEGs were identified using the limma package, with thresholds set at $|\log_2 \text{fold change}| > 0.5$ and adjusted $P < 0.05$. Overlapping DEGs between DFU and AS were visualized using Venn diagrams. Gene Ontology (GO) and Kyoto Encyclopedia of Genes and Genomes (KEGG) pathway enrichment analyses were performed on the overlapping genes using the clusterProfiler package.

Machine Learning and Feature Gene Selection

Three machine learning algorithms were applied to screen core feature genes from the senescence-related DEGs. (1) LASSO regression with 10-fold cross-validation was performed using the glmnet package. The optimal penalty parameter λ was determined by the minimum binomial deviance. (2) Random forest (RF) analysis was carried out with the randomForest package (ntree = 500); variable importance was ranked by mean decrease Gini, and genes with importance scores above a threshold were retained. (3) Support vector machine-recursive feature elimination (SVM-RFE) was implemented using the e1071 package with a linear kernel, and 10-fold cross-validation was used to select the optimal feature subset. The intersection of genes identified by the three algorithms yielded the final feature genes.

Construction and Validation of Diagnostic Model

A multi-gene diagnostic nomogram was constructed using the rms package in R based on the selected feature genes. The area under the receiver operating characteristic curve (AUC) was calculated with the pROC package to evaluate diagnostic performance. Calibration curves were generated to assess the agreement between predicted and observed outcomes. Decision curve analysis (DCA) was performed using the rmda package to evaluate the clinical net benefit of the nomogram. External validation was conducted using independent datasets (GSE134431 for DFU and GSE163154 for AS).

Single-Cell RNA Sequencing Data Analysis

Raw single-cell RNA-seq data were imported and preprocessed using the Seurat package (v5.2.1). Quality control filters removed cells with nFeature_RNA ≤ 300 and genes detected in fewer than five cells, retaining 42,989 high-quality cells for subsequent analyses. The filtered expression matrix was normalized, and principal component analysis (PCA) was applied to reduce dimensionality. Unsupervised clustering was conducted using the UMAP algorithm (resolution = 0.6), resolving 20 discrete cell clusters. Final cell-type annotation integrated canonical marker expression profiles with reference-based annotation leveraging the ACT database (http://xteam.xbio.top/ACT/), yielding 14 major cell lineages.

Clinical Tissue Sample Validation

DFU and nDFU tissue samples were collected with informed consent. Immunohistochemistry (IHC) was performed using primary antibodies against p21, γH2AX, HMGB1, and p16, followed by HRP-conjugated secondary antibodies and DAB visualization. Senescence-associated β-galactosidase (SA-β-gal) staining was performed using a commercial kit (Beyotime, China). Total RNA was extracted using TRIzol reagent, reverse transcribed with HiScript III RT SuperMix, and qRT-PCR was performed using SYBR Green Master Mix. Primer sequences are listed in Supplementary Table S1.

Primary Isolation and Treatment of Human Dermal Fibroblasts

Primary human dermal fibroblasts were isolated from skin tissue of non-diabetic control patients undergoing surgical debridement with informed consent. The study was approved by the Scientific Research Ethics Committee of General Hospital of Southern Theater Command, PLA (approval No. NZLLKZ2026060). Fresh skin tissues were minced and digested with trypsin-EDTA and collagenase type I, and cells were cultured in DMEM with 10% FBS. Fibroblasts at passages 3–6 were treated with 4.5 g/L glucose plus 200 μM palmitic acid (HGHL) or 500 μM H_2O_2 for 24 hours to induce senescence. Metformin (200 μM) was added for 24 hours. Control cells were cultured in normal glucose DMEM (1.5 g/L). All experiments were performed in triplicate and repeated at least three times independently.

Western Blotting

Cells or tissue samples were lysed in RIPA buffer supplemented with protease and phosphatase inhibitors. Protein concentrations were determined using the BCA assay. Equal amounts of protein (30 μg) were separated by SDS-PAGE and transferred onto PVDF membranes. Membranes were blocked with 5% non-fat milk and then incubated overnight at 4°C with primary antibodies against p16, p21 and β-actin (loading control). After washing, membranes were incubated with HRP-conjugated secondary antibodies for 1 h at room temperature. Bands were visualized using enhanced chemiluminescence (ECL) and quantified using ImageJ software.

Statistical Analysis

All statistical analyses were performed using R software (version 4.2.3) or GraphPad Prism 9.0. Data are presented as mean ± standard deviation (SD). Comparisons between two groups were performed using two-tailed Student's t-test or Mann-Whitney U test, as appropriate. Comparisons among three or more groups were performed using one-way ANOVA followed by Tukey's post hoc test. Correlation analyses were conducted using Spearman's rank correlation coefficient. A P value < 0.05 was considered statistically significant. All experiments were repeated at least three times independently.

Declarations

Consent to participate:

Informed consent was obtained from all individual participants included in this study.

Ethics approval and consent to participate:

All procedures performed in this study involving human participants were in accordance with the ethical standards of the institutional research committee and with the 1964 Helsinki declaration and its later amendments. The study protocol was approved by the Scientific Research Ethics Committee of General Hospital of Southern Theater Command, PLA (approval No. NZLLKZ2026060). Informed consent was obtained from all individual participants included in this study.

Funding:

This research was funded by the Mid-Career Talent Program of General Hospital of Southern Theater Command.

Author Contribution

Conceptualization, F.Z. and J.C.; methodology, F.Z.; software, H.W. and Y.Y.; validation, F.Z. and H.W.; formal analysis, H.W.; investigation, Y.Y., C.L., and X.W.; resources, J.C.; data curation, F.Z. and Y.Y.;

writing—original draft preparation, F.Z.; writing—review and editing, F.Z., H.W., Y.Y., C.L., X.W., J.C., and T.Z.; visualization, H.W.; supervision, J.C. and T.Z.; project administration, J.C.; funding acquisition, J.C. All authors have read and agreed to the published version of the manuscript.

Acknowledgement

We thank the Department of Burn and Plastic Surgery, General Hospital of Southern Theater Command—a PLA Key Clinical Specialty (Plastic Surgery) and a High-Quality Discipline of the PLA Joint Logistics Support Force—for providing clinical tissue samples and technical support.

Data Availability

The transcriptomic datasets GSE134431, GSE163154, and GSE245703 analyzed in this study are publicly available in the Gene Expression Omnibus (GEO) database (https://www.ncbi.nlm.nih.gov/geo/). The senescence-associated gene set was retrieved from the CellAge database (https://genomics.senescence.info/cells/). No new sequencing data were generated in this study. The clinical tissue sample data generated during this study are not publicly available due to patient privacy and ethical restrictions but are available from the corresponding author upon reasonable request. The study protocol was approved by the Scientific Research Ethics Committee of General Hospital of Southern Theater Command, PLA (approval No. NZLLKZ2026060).

References

1. Sun H et al (2022) IDF Diabetes Atlas: Global, Regional and Country-Level Diabetes Prevalence Estimates for 2021 and Projections for 2045. Diabetes Res Clin Pract 183:109119. 10.1016/j.diabres.2021.109119
2. Armstrong DG et al (2023) Diabetic Foot Ulcers: A Review. JAMA, vol. 330, no. 1, pp. 62–75. 10.1001/jama.2023.10578
3. Libby P (2021) The Changing Landscape of Atherosclerosis. Nature 592(7855):524–533. 10.1038/s41586-021-03392-8
4. Lilja M et al (2018) Risk of Lower Extremity Artery Disease in Type 2 Diabetes: A Swedish Cohort Study. Diabetes Care. 41(10):2157–2164. 10.2337/dc18-0485
5. Pal R, Sanjay K, Bhadada (2023) AGEs accumulation with vascular complications, glycemic control and metabolic syndrome: A narrative review. Bone. 176:116884. 10.1016/j.bone.2023.116884
6. Silveira Rossi L et al Metabolic syndrome and cardiovascular diseases: Going beyond traditional risk factors. Diabetes/metabolism research and reviews vol. 38,3 (2022): e3502. 10.1002/dmrr.3502
7. López-Otín C et al (2023) Hallmarks of Aging: An Expanding Universe. Cell, vol. 186, no. 2, pp. 243–278. 10.1016/j.cell.2022.11.001

8. Palmer AK et al (2015) Cellular Senescence in Type 2 Diabetes: A Therapeutic Opportunity. Diabetes. 64:2289–2298. 10.2337/db14-1820
9. Tabas I et al (2015) Recent insights into the cellular biology of atherosclerosis. J cell biology vol 209(1):13–22. 10.1083/jcb.201412052
10. Ogrodnik M et al (2017) Cellular senescence drives age-dependent hepatic steatosis. Nature communications vol. 8 15691. 13 Jun. 10.1038/ncomms15691
11. Chiu C-C et al (2023) Prolonged Exposure to High Glucose Induces Premature Senescence Through Oxidative Stress and Autophagy in Retinal Pigment Epithelial Cells. Archivum immunologiae et therapiae experimentalis vol. 71,1 21. 28 Aug. 10.1007/s00005-023-00686-9
12. Liu J et al (2024) Cellular Senescence: A Bridge Between Diabetes and Microangiopathy. Biomolecules 14,11 1361. 25 Oct. 10.3390/biom14111361
13. Grootaert MOJ (2024) Cell senescence in cardiometabolic diseases. npj aging vol. 10,1 46. 21 Oct. 10.1038/s41514-024-00170-4
14. Childs BG Senescent intimal foam cells are deleterious at all stages of atherosclerosis., Science et al (2016) (New York, N.Y.) vol. 354,6311 : 472–477. 10.1126/science.aaf6659
15. Samarawickrama PN et al (2024) Clearance of senescent cells enhances skin wound healing in type 2 diabetic mice. Theranostics. 26 Aug 14:14 5429–5442. 10.7150/thno.100991
16. Ali I et al (2024) Understanding the intricacies of cellular senescence in atherosclerosis: Mechanisms and therapeutic implications. Ageing Res Rev 96:102273. 10.1016/j.arr.2024.102273
17. Steegen L, Mandy OJ, Grootaert (2026) Senescence as a Driver of Smooth Muscle Cell Plasticity and Atherosclerosis: Mechanisms and Therapeutic Opportunities. Cells vol. 15,2 114. 8 Jan. 10.3390/cells15020114
18. Wilkinson HN, Matthew J, Hardman (2020) Senescence in Wound Repair: Emerging Strategies to Target Chronic Healing Wounds. Front Cell Dev Biology 8:773. 10.3389/fcell.2020.00773
19. Ueda N et al (2026) The role of cellular senescence in wound healing of diabetic skin. J Biochem vol 179(4):241–248. 10.1093/jb/mvag006
20. Lundberg AS, Weinberg RA (1998) Functional inactivation of the retinoblastoma protein requires sequential modification by at least two distinct cyclin-cdk complexes. Mol Cell biology vol 18(2):753–761. 10.1128/MCB.18.2.753
21. He S, Norman E, Sharpless (2017) Senescence in Health and Disease. Cell. 169(6):1000–1011. 10.1016/j.cell.2017.05.015
22. Longhurst AD et al (2025) The PRC2.1 subcomplex opposes G1 progression through regulation of CCND1 and CCND2. eLife. 4 Feb 13 RP97577. 10.7554/eLife.97577
23. Dulić V et al (2000) Uncoupling between phenotypic senescence and cell cycle arrest in aging p21-deficient fibroblasts. Mol Cell biology vol 20:6741–6754. 10.1128/MCB.20.18.6741-6754.2000
24. Chen W et al (2022) Multiple functions of CALCOCO family proteins in selective autophagy. J Cell Physiol vol 237(9):3505–3516. 10.1002/jcp.30836

25. Shan W et al (2025) Targeting mitochondrial autophagy for anti-aging. Cell death discovery vol. 12,1 78. 24 Dec. 10.1038/s41420-025-02913-y
26. Bahar ME et al (2026) The autophagy-senescence axis as a threshold model of aging and therapeutic targeting. Redox Biol 91:104079. 10.1016/j.redox.2026.104079
27. Song F-C et al (2022) High glucose represses the proliferation of tendon fibroblasts by inhibiting autophagy activation in tendon injury. Bioscience Rep vol 42(3):BSR20210640. 10.1042/BSR20210640
28. Kurz DJ et al (2000) Senescence-associated (beta)-galactosidase reflects an increase in lysosomal mass during replicative ageing of human endothelial cells. J Cell Sci 113:3613–3622 (Pt 20). 10.1242/jcs.113.20.3613
29. Listinsky JJ et al (1998) Alpha-L-fucose: a potentially critical molecule in pathologic processes including neoplasia. Am J Clin Pathol vol 110(4):425–440. 10.1093/ajcp/110.4.425
30. Kulkarni AS et al (2020) Benefits of Metformin in Attenuating the Hallmarks of Aging. Cell Metabolism, vol. 32, no. 1, pp. 15–30. 10.1016/j.cmet.2020.04.001
31. Wang Y et al (2019) Metformin Improves Mitochondrial Respiratory Activity through Activation of AMPK. Cell Reports. 29(6):1511–1523e5. 10.1016/j.celrep.2019.09.070
32. Yang Y et al (2024) Metformin decelerates aging clock in male monkeys. Cell. 187(22):6358–6378e29. 10.1016/j.cell.2024.08.021
33. Qiu X et al (2021) Metformin alleviates β-glycerophosphate-induced calcification of vascular smooth muscle cells via AMPK/mTOR-activated autophagy. Experimental therapeutic Med vol 21(1):58. 10.3892/etm.2020.9490
34. Wang S et al (2022) Circulating Exosomal miR-181b-5p Promoted Cell Senescence and Inhibited Angiogenesis to Impair Diabetic Foot Ulcer via the Nuclear Factor Erythroid 2-Related Factor 2/Heme Oxygenase-1 Pathway. Frontiers in cardiovascular medicine vol. 9 844047. 20 Apr. 10.3389/fcvm.2022.844047

Figures

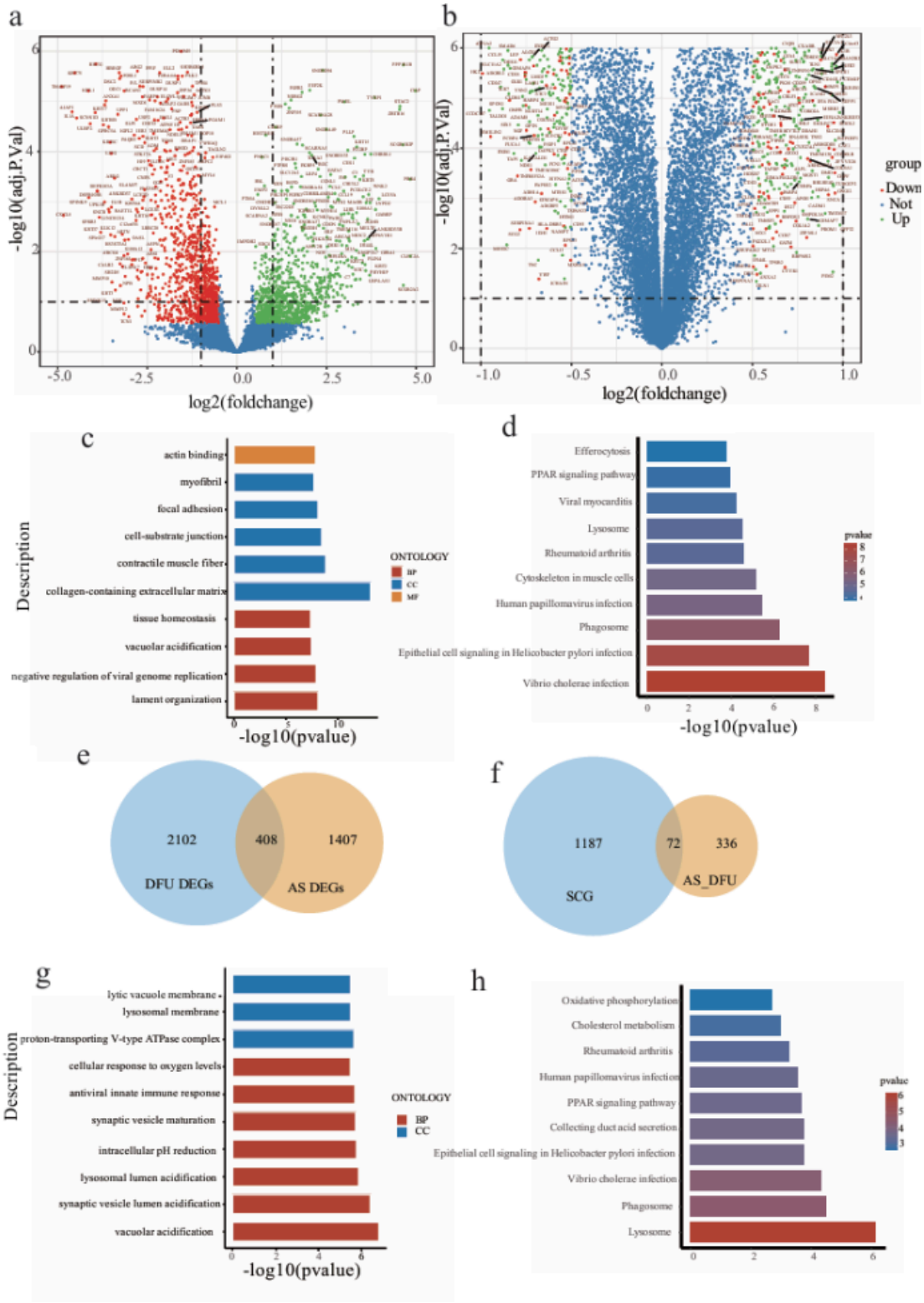


Figure 1

Cellular senescence is a common pathological feature of diabetic foot and atherosclerosis.

(a, b) Volcano plots showing differentially expressed genes (DEGs) in DFU (GSE134431, a) and AS (GSE163154, b) compared with healthy controls. Red and green dots represent upregulated and downregulated genes, respectively ($|\log_2 FC| > 1$, adjusted $P < 0.05$). (c) Gene Ontology (GO) enrichment

analysis of the 408 genes commonly dysregulated in both DFU and AS. (d) Kyoto Encyclopedia of Genes and Genomes (KEGG) pathway enrichment analysis of the 408 common DEGs. (e) Venn diagram illustrating the overlap of DEGs between DFU and AS. (f) Identification of senescence-related DEGs (SR-DEGs) by intersecting the 408 common DEGs with the CellAge senescence-associated gene set. (g, h) GO (g) and KEGG (h) enrichment analyses of the 72 SR-DEGs. Statistical significance was determined using the moderated t-test with Benjamini-Hochberg correction. Adjusted P < 0.05 was considered significant. KEGG pathway maps used in this figure are reproduced with permission from the Kanehisa Laboratories (https://www.kegg.jp/).

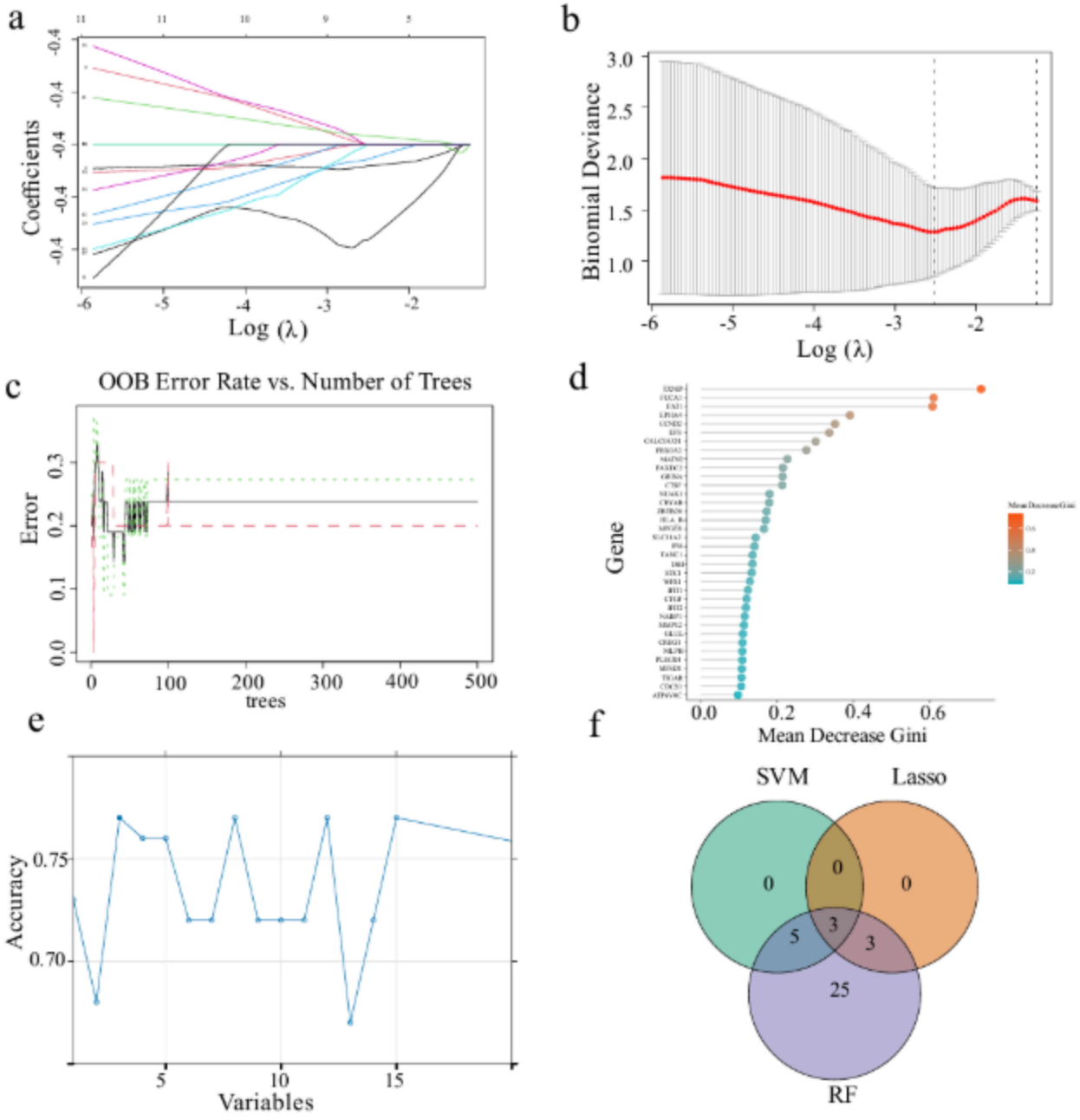


Figure 2

Machine learning identifies three core feature genes.

(a, b) LASSO regression analysis with 10-fold cross-validation. (a) Coefficient profiles of the 72 senescence-related DEGs as a function of the penalty parameter λ. (b) Binomial deviance plot for cross-validation; the optimal λ value (0.014) is indicated by the dotted vertical line. (c, d) Random forest (RF) analysis. (c) Error rate versus number of trees. (d) Variable importance ranking based on mean decrease Gini; the top 36 genes are shown. (e) Support vector machine-recursive feature elimination (SVM-RFE) analysis showing the accuracy of different feature subsets; the optimal subset containing 8 genes is indicated. (f) Venn diagram showing the intersection of genes selected by LASSO, RF, and SVM-RFE, yielding three core feature genes: CALCOCO1, CCND2, and FUCA1.

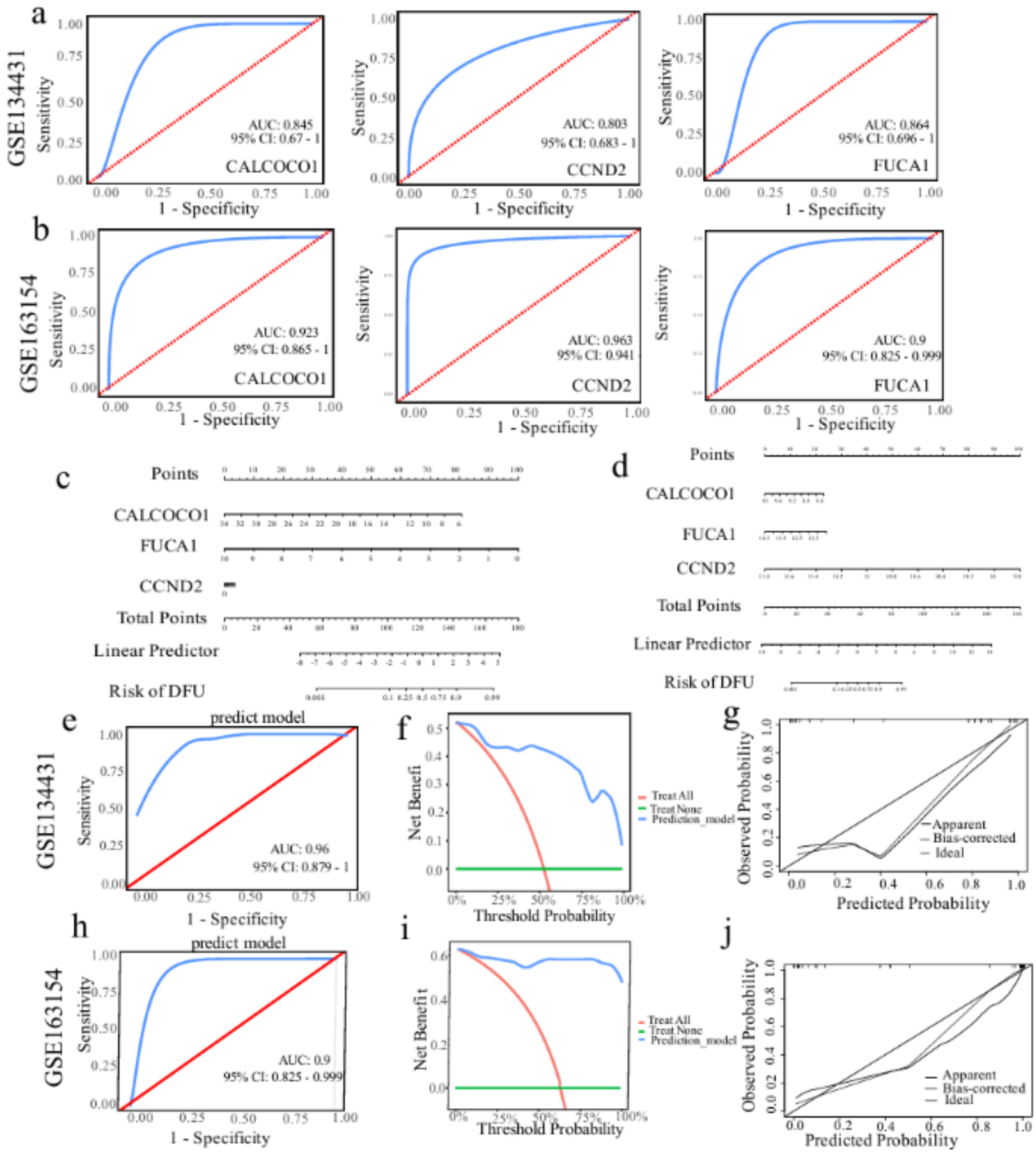


Figure 3

A multi-gene diagnostic model exhibits excellent performance in both diseases.

(a, b) Receiver operating characteristic (ROC) curves of CALCOCO1, CCND2, and FUCA1 for discriminating DFU patients from healthy controls in GSE134431 (a) and AS patients from healthy controls in GSE163154 (b). AUC values are indicated. (c, d) Nomogram for predicting DFU risk (c) and AS risk (d) based on the three feature genes. Points are assigned to each gene according to its expression

level; the total points predict the probability of disease. (e, h) ROC curves of the multi-gene nomogram in the DFU dataset (AUC = 0.96, 95% CI: 0.879–1.000; e) and the AS dataset (AUC = 0.90, 95% CI: 0.825–0.999; h). (f, i) Decision curve analysis (DCA) demonstrating the net clinical benefit of the nomogram in DFU (f) and AS (i). (g, j) Calibration curves showing agreement between predicted probabilities and observed outcomes in DFU (g) and AS (j).

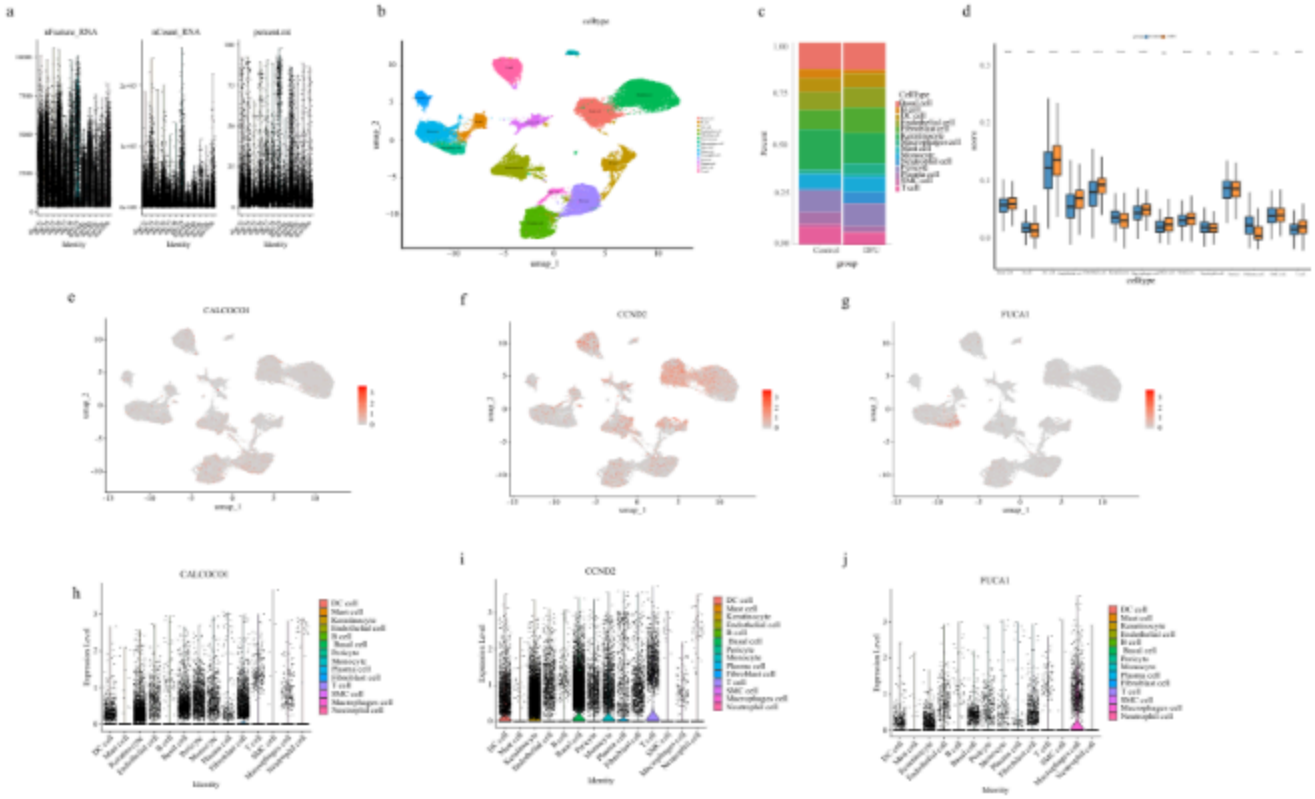


Figure 4

Feature genes display cell type–specific expression patterns within diabetic foot tissue.

(a) Quality control metrics of single-cell RNA sequencing: violin plots displaying the distribution of detected genes (nFeature_RNA), total UMI counts (nCount_RNA), and mitochondrial gene expression percentage (percent.mt) across samples. (b) UMAP visualization of cells colored by annotated cell types; distinct colors distinguish different cell subpopulations. (c, d) Proportions of major cell types in DFU and nDFU (non-diabetic foot ulcer) skin tissues (c) and statistical comparison of cell type proportions (d). P < 0.05, *P < 0.01, **P < 0.001 (Wilcoxon rank-sum test). (e–g) Feature plots showing the spatial distribution of CALCOCO1 (e), CCND2 (f), and FUCA1 (g) expression in UMAP space. (h–j) Violin plots showing the expression distribution of CALCOCO1 (h), CCND2 (i), and FUCA1 (j) across major cell types, including fibroblasts, pericytes, keratinocytes, basal cells, macrophages, monocytes, and endothelial cells. P < 0.05, *P < 0.01, **P < 0.001 (Wilcoxon rank-sum test).

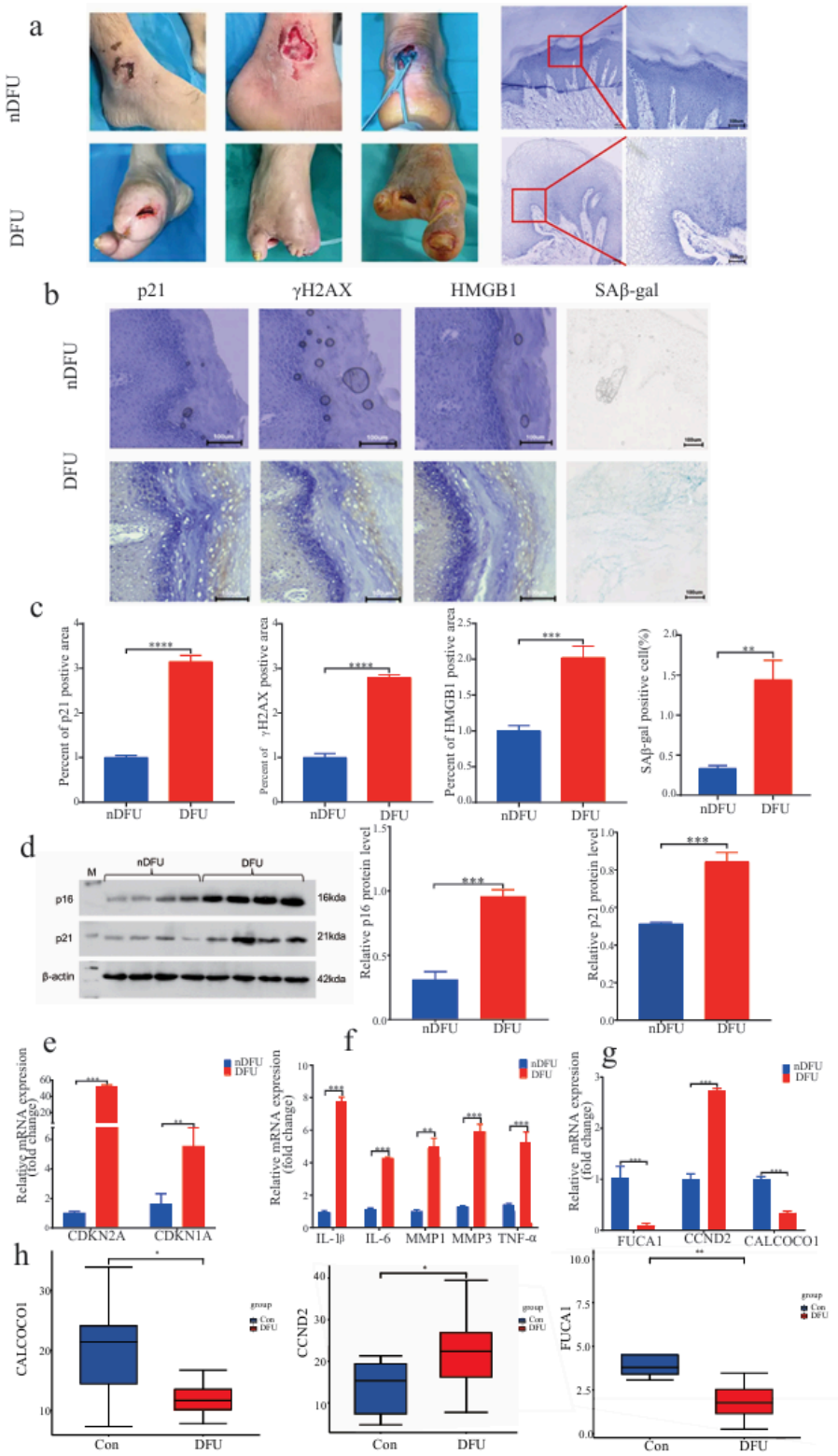


Figure 5

Senescent cells accumulate in diabetic foot ulcer tissues.

(a) Representative H&E staining images of clinical tissue samples from nDFU (non-diabetic foot ulcer) and DFU patients. Scale bar = 100 μm. (b) Representative immunohistochemical (IHC) staining of senescence markers p21, γH2AX, and HMGB1, as well as SA-β-gal staining, in nDFU and DFU tissues.

Scale bar = 100 μm. (c) Quantification of IHC staining and SA-β-gal-positive cells in nDFU and DFU tissues. (d) Western blot analysis of p16 and p21 protein levels in nDFU and DFU tissues; β-actin serves as loading control. (e) Relative mRNA expression of p16 and p21 determined by qRT-PCR. (f) Relative mRNA expression of SASP factors (IL-1β, IL-6, MMP1, MMP3, TNF-α) in DFU vs. nDFU tissues. (g) Relative mRNA expression of CALCOCO1, CCND2, and FUCA1 in DFU vs. nDFU tissues. (h) Relative mRNA expression of CALCOCO1, CCND2, and FUCA1 in the GSE134431 dataset. Data are presented as mean ± SD. P < 0.05, *P < 0.01, **P < 0.001 (two-tailed Student's t-test). Full-length blots are presented in Supplementary Fig. S1.

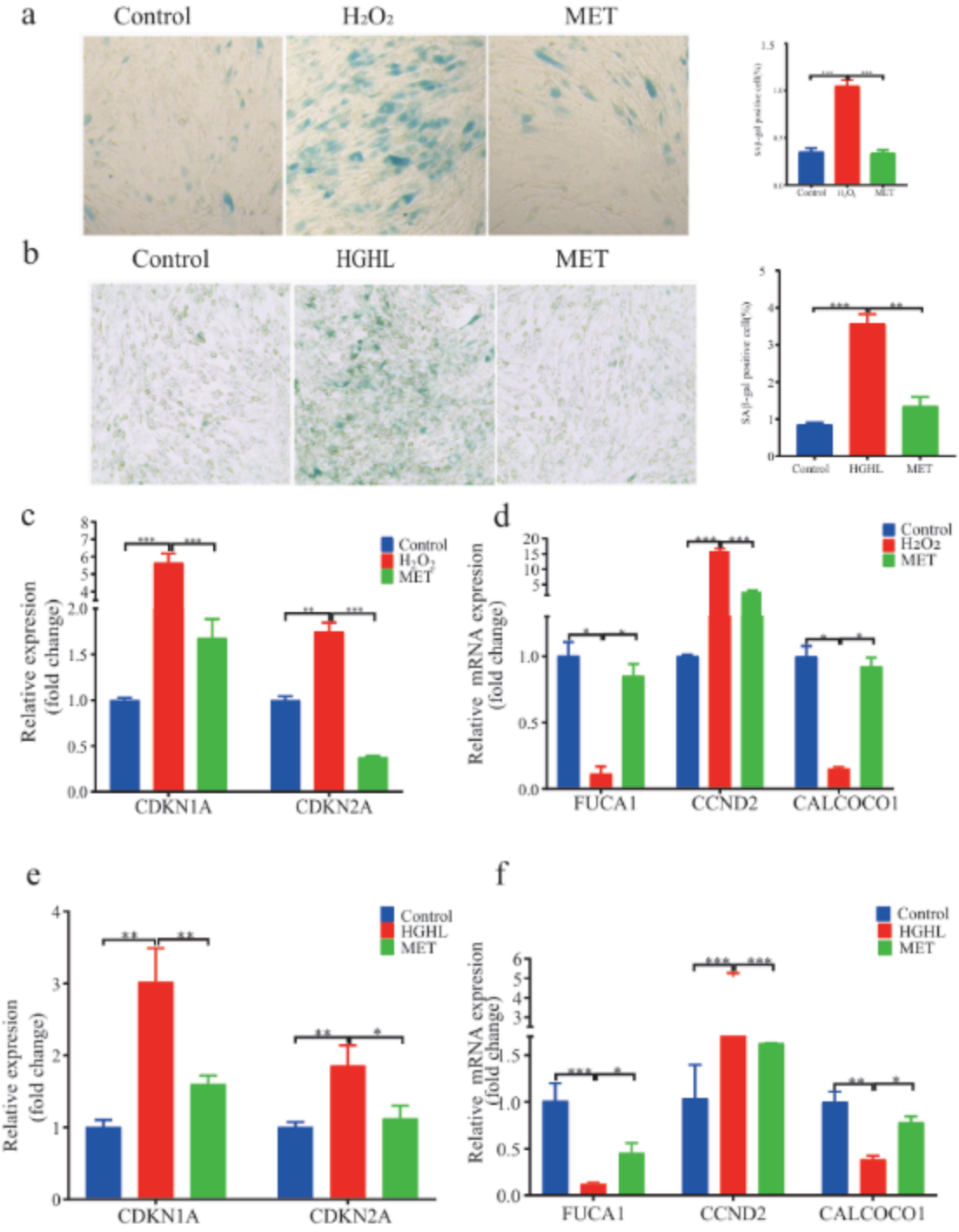


Figure 6

Metformin attenuates fibroblast senescence in vitro.

(a) Representative SA-β-gal staining images and quantification of SA-β-gal-positive cells in human primary dermal fibroblasts treated with H_2O_2 (500 μM) alone or in combination with metformin (Met, 200 μM). Scale bar = 100 μm. (b) Representative SA-β-gal staining images and quantification of SA-β-gal-positive cells in human primary dermal fibroblasts treated with high glucose (4.5 g/L) combined with high lipid (HGHL, 200 μM palmitic acid) alone or in combination with metformin (Met, 200 μM). (c, d) Relative mRNA expression of CDKN1A (p21), CDKN2A (p16), CALCOCO1, CCND2, and FUCA1 in fibroblasts treated with H_2O_2 with or without metformin, determined by qRT-PCR. (e, f) Relative mRNA expression of CDKN1A (p21), CDKN2A (p16), CALCOCO1, CCND2, and FUCA1 in fibroblasts treated with HGHL with or without metformin, determined by qRT-PCR. Data are presented as mean ± SD from three independent experiments. $P < 0.05$, *$P < 0.01$, **$P < 0.001$ (one-way ANOVA with Tukey's post hoc test).